TELLING PLANETS FROM SPECKLES CREATED BY TELESCOPE SEGMENTATION

Natalia Yaitskova[1] and Szymon Gladysz

European Organization for Astronomical Research in the Southern Hemisphere

Karl Schwarzschildstr. 2 D-85748 Garching bei Muenchen, Germany, [1]nyaitsko@eso.org

ABSTRACT

Segmentation of telescope's primary mirror creates quasi-static speckles in an image. These speckles are impediment for the detection of faint structures around stars, for instance exoplanets. An elaborated post-processing method is required to improve the detection level. The Stochastic Speckle Discrimination (SSD) method developed for this purpose uses statistical variability of intensity to distinguish between planets and speckles. To calculate the efficiency of SSD we derive analytical expressions for mean and standard deviation of point spread function (PSF) produced by segmented pupil. The expressions are general for any point in the image plane, but there is a difference in statistical behavior for the central point and for the off-axis point. In particular we show that a modified Rician distribution is inapplicable to describe on-axis intensity. In the last section we calculate the level of primary mirror phasing required for the efficient use of SSD.

Keywords: speckles, statistical optics, ELT, segmentation, high-contrast imaging

1. INTRODUCTION

Primary mirrors of some large modern telescopes consist of segments. Depending on the diameter of the primary, the number of segments varies from 36 (Keck[1] , GTC[2]) to 800-1000 (EELT[3], TMT[4]). The segments constantly move; they shift in the direction outside the optical surface (piston, tip and tilt aberrations in terms of Zernike polynomials) creating a randomly blazed diffraction grating.[5] Image formed by such a grating is diffraction pattern plus a field of random speckles (Figure 1). The active control (phasing) reduces the amplitude of the segments' shifts but there are always some residuals. As segments move the image pattern changes, but as these movements are slow (compared to the changes caused by the turbulent atmosphere) we speak about quasi-static speckles. These speckles are not fast enough to be averaged-out by long exposures, and are not static enough to be removed by calibration. Size of the speckle is defined by the primary mirror diameter, as well as the size of any non-resolved object. The quasi-static speckle looks pretty much like a non-resolved companion and can be mistaken for one.

Several facts help distinguish between a speckle and an object. Firstly, the object rotates with the field and speckles rotate with the pupil. This is the principle of the angular differential imaging method for detection of exoplanets. Secondly, spectral features of the object are different from the parent star's and hence from the speckle's. Spectral differential imaging relies on this difference. Thirdly, as we already mentioned, speckle fluctuates more than the object. This is the principle of stochastic speckle discrimination (SSD)[6], which we consider throughout this paper.

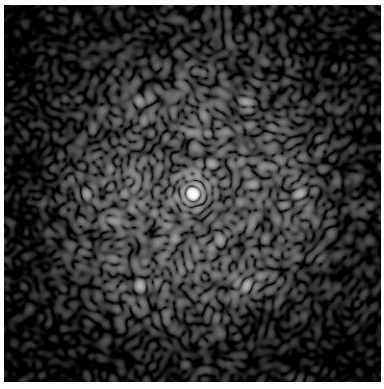

Figure 1. Simulated "instantaneous" image from a segmented telescope: central core, speckles and diffraction peaks.

If the mirror is completely de-phased (amplitude of the segment shift is close to the imaging wavelength), the image consists of speckles only, and the central core disappears. Obviously in this case the central pixel of the PSF fluctuates as much as any other pixel and statistics-based discrimination is inapplicable. The question we want to answer in this paper is: Up to which level of phasing is the SSD method efficient? For that we have to derive not only the mean value of the PSF, but also the measure of its fluctuation, i.e. standard deviation.

Ground-based and Airborne Telescopes III, edited by Larry M. Stepp, Roberto Gilmozzi, Helen J. Hall
Proc. of SPIE Vol. 7733, 773351 · © 2010 SPIE · CCC code: 0277-786X/10/$18 · doi: 10.1117/12.856112

2. STATISTICAL MOMENTS OF INTENSITY

2.1. Mean value

We consider a segmented pupil composed of N identical segments. For simplicity we assume that segments have random piston values. The complex amplitude in the image plane is:[5,7]

$$U(\boldsymbol{w}) = t(\boldsymbol{w}) \cdot \frac{1}{N} \sum_{j=1}^{N} \exp(ik\boldsymbol{w}\boldsymbol{r}_j) \exp(i\delta_j) \tag{1}$$

where $t(\boldsymbol{w})$ is a complex amplitude of one segment, $\boldsymbol{w}$ is a coordinate in the image plane, $\boldsymbol{r}_j$ is position of the center of a segment with index j, δ_j is phase value associated with segment j, and k is the wavenumber. Intensity is the modulus square of the function $U(\boldsymbol{w})$. Assuming δ_j to be independent and identically distributed (i.i.d.) the mean of intensity is a sum of normalized PSF from a perfect pupil, $I_c(\boldsymbol{w})$, and a halo $I_s(\boldsymbol{w})$:

$$\langle I \rangle(\boldsymbol{w}) = I_c(\boldsymbol{w}) + I_s(\boldsymbol{w}). \tag{2}$$

Here $\langle ... \rangle$ represents statistical mean and

$$I_c(\boldsymbol{w}) = a_1^2 |gf(\boldsymbol{w})|^2 |t(\boldsymbol{w})|^2, \qquad I_s(\boldsymbol{w}) = \frac{1 - a_1^2}{N} |t(\boldsymbol{w})|^2, \tag{3}$$

where $a_1 = \langle \exp(i\delta_j) \rangle$ and

$$gf(\boldsymbol{w}) = \frac{1}{N} \sum_{j=1}^{N} \exp(ik\boldsymbol{w}\boldsymbol{r}_j) \tag{4}$$

is the Fourier transform of segmentation grid – a grid factor. Notice than in absence of phase errors $a_1 = 1$, halo disappears $I_s(\boldsymbol{w}) = 0$, and $I_c(\boldsymbol{w})$ becomes the PSF from a perfect pupil $I_c(\boldsymbol{w}) = |gf(\boldsymbol{w})|^2 |t(\boldsymbol{w})|^2$. Functions $|t(\boldsymbol{w})|^2$ and $|gf(\boldsymbol{w})|^2$ are shown in Figure 2 for one-dimensional telescope. Functions $gf(\boldsymbol{w})$ and $t(\boldsymbol{w})$ are normalized such that at the central point $gf(0) = t(0) = 1$, so that the mean intensity at the central point is:

$$\langle I \rangle(0) = a_1^2 + \frac{1 - a_1^2}{N}. \tag{5}$$

This value is often associated with the Strehl ratio.[5] Parameter a_1 depends on the statistical distribution of δ_j. If δ_j are normally distributed with zero mean and standard deviation σ then $a_1 = \exp(-\sigma^2/2)$; for uniform distribution in interval $\left[-\sigma\sqrt{3},\ \sigma\sqrt{3}\right]$ $a_1 = \mathrm{sinc}(\sqrt{3}\sigma)$. If δ_j are distributed uniformly between $\pm\pi$ (for Gaussian distribution it means that $\sigma >> 1$) $a_1 = 0$ and $\langle I \rangle$ turns into PSF of a fully de-phased pupil:

$$\langle I \rangle \to \frac{|t(\boldsymbol{w})|^2}{N}. \tag{6}$$

Representation of mean intensity as a sum of two terms (Eq.(2)) is valid for any statistical distribution of δ_j and for any number of segments. The values δ_j do not need to be small or large. The only assumption made is the i.i.d. nature of the segments' aberrations.

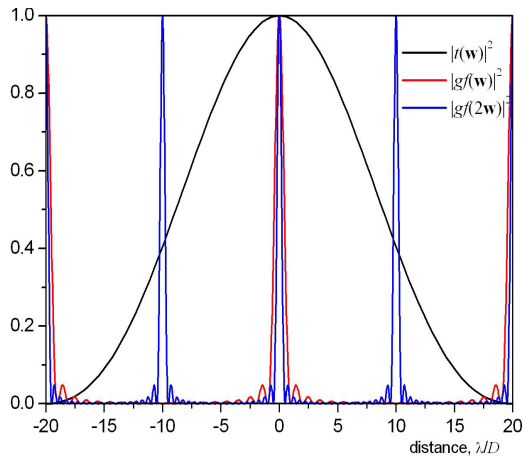

Figure 2. Functions included in expressions for the moments. *D* – pupil diameter, λ - wavelength, *N*=20

2.2. Standard deviation

To derive standard deviation of intensity one has to calculate averages from a quadruple sum:

$$\sum_{j=1}^{N}\sum_{m=1}^{N}\sum_{p=1}^{N}\sum_{q=1}^{N}\exp\left(-ik\boldsymbol{w}\boldsymbol{r}_q\right)\exp\left(ik\boldsymbol{w}\boldsymbol{r}_p\right)\exp\left(-ik\boldsymbol{w}\boldsymbol{r}_m\right)\exp\left(ik\boldsymbol{w}\boldsymbol{r}_j\right)\left\langle\exp\left(-i\delta_q\right)\exp\left(i\delta_p\right)\exp\left(-i\delta_m\right)\exp\left(i\delta_j\right)\right\rangle \tag{7}$$

According to Appendix B of classic book by Goodman[8] 15 cases must be considered to calculate the averages like Eq.(7). Our situation is somehow more complicated than the one from the afore-mentioned book because Eq.(7) contains field-dependant terms $\exp\left(ik\boldsymbol{w}\boldsymbol{r}_j\right)$. Following Goodman's scheme we have made this exercise and arrived at the final expression:

$$\sigma_I^2(\boldsymbol{w})=\frac{|t(\boldsymbol{w})|^4}{N}\left[\frac{\alpha_0}{N}+\alpha_1|gf(\boldsymbol{w})|^2+\alpha_2|gf(2\boldsymbol{w})|^2+\alpha_3|gf(\boldsymbol{w})|^2 gf(2\boldsymbol{w})\right] \tag{8}$$

where

$$\begin{aligned}\alpha_0&=\left(1-a_1^2\right)^2+\frac{2\left(a_2-a_1^4\right)-\left[\left(1+a_2\right)-2a_1^2\right]^2}{N},\\ \alpha_1&=2a_1^2\left\{1-a_1^2-\frac{2\left[\left(1+a_2\right)-2a_1^2\right]}{N}\right\},\\ \alpha_2&=\frac{\left(a_2-a_1^2\right)^2}{N},\qquad \alpha_3=2a_1^2\left(a_2-a_1^2\right).\end{aligned} \tag{9}$$

Functions $|t(\boldsymbol{w})|^2$, $|gf(\boldsymbol{w})|^2$ and $|gf(2\boldsymbol{w})|^2$ are shown in Figure 2. A new parameter appeared:

$$a_2=\left\langle\exp\left(i2\delta_j\right)\right\rangle. \tag{10}$$

For normal distribution $a_2=\exp(-2\sigma^2)=a_1^4$; for uniform distribution $a_2=\operatorname{sinc}\left(2\sqrt{3}\sigma\right)$.

For the central peak $gf(0)=t(0)=1$ and Eq.(8) gives:

$$\begin{aligned}\sigma_I^2(0)&=\frac{1}{N}\left(\frac{\alpha_0}{N}+\alpha_1+\alpha_2+\alpha_3\right)\\ &=\frac{N-1}{N^3}\left[1+2a_1^2(N-2)(a_2+1)+a_2^2-2a_1^4(2N-3)\right].\end{aligned} \tag{11}$$

The result for $\sigma_I(0)$ coincides with the expressions (3-91)-(3-92) form the Reference[8] if one sets all lengths of random phasors to $1/\sqrt{N}$.

Now, let us restrict the phase distribution to normal and express $\sigma_I^2(\boldsymbol{w})$ through I_c and I_s. With the help of identity $\left(1+a_2\right)-2a_1^2=\left(1-a_1^2\right)^2$, which is valid for normal distribution, the combination of terms yields:

$$\sigma_I^2(\boldsymbol{w})=I_s^2(\boldsymbol{w})\left[1-N\left(\frac{1-a_1^2}{N}\right)^2\right]+2I_c(\boldsymbol{w})I_s(\boldsymbol{w})\left(1-2\frac{1-a_1^2}{N}\right)+I_c^2(\boldsymbol{w})\left(1-\frac{1-a_1^2}{N}\frac{gf(2\boldsymbol{w})}{|gf(\boldsymbol{w})|^2}\right)^2-I_c^2(\boldsymbol{w}). \tag{12}$$

We have assumed that for symmetric pupils $gf(2\boldsymbol{w})$ is real and therefore $|gf(2\boldsymbol{w})|^2=gf^2(2\boldsymbol{w})$. For $\sigma>>1$:

$$\sigma_I(\boldsymbol{w})\to\frac{|t(\boldsymbol{w})|^2}{N}\sqrt{1-\frac{1}{N}}. \tag{13}$$

In this limit the speckle *contrast* is independent of the position in the focal plane:

$$C=\frac{\sigma_I(\boldsymbol{w})}{\langle I\rangle(\boldsymbol{w})}\to\sqrt{1-\frac{1}{N}}. \tag{14}$$

as it must be for the developed speckles with a finite number of phasors.[9]

Expression (12) contains many terms and in the next sub-section we will simplify it. The location under investigation $\boldsymbol{w}$ dictates the manner of simplification which is different for the central point and the diffraction peaks compared to the other locations.

2.3. Approximations for σ_I

2.3.1. *Beyond the central point and the diffraction peaks*

Outside the peaks (cf. Figure 2) functions $|gf(\boldsymbol{w})|^2$ and $I_c(\boldsymbol{w})$ decrease as N^{-2} with the number of segments. In Eq.(12) we neglect all terms which decrease faster than N^{-3}, i.e. all terms containing N^{-4}:

$$\sigma_I^2(\boldsymbol{w}) \approx I_s^2(\boldsymbol{w})\left[1-\frac{\left(1-a_1^2\right)^2}{N}\right]+2I_c(\boldsymbol{w})I_s(\boldsymbol{w}). \quad \text{(“approximation 1”)} \tag{15}$$

For small standard deviation of phase σ or for large N the second term in rectangular brackets can be neglected and the expression becomes identical to the one derived from the modified Rician distribution

$$\sigma_I^2(\boldsymbol{w}) \approx I_s^2(\boldsymbol{w})+2I_s(\boldsymbol{w})I_c(\boldsymbol{w}). \quad \text{(“Rician approximation”)} \tag{16}$$

Modified Rician distribution describes statistics of intensity for a random phasor sum plus a constant phasor. It was derived for the case of infinite number of phasors.[8] In our case the number of segments is limited. Figure 3 shows standard deviation calculated by exact expression, by approximation 1, Eq.(15), and the Rician approximation, Eq.(16).

Figure 3 left panel: even for relatively small number of segments there is a good agreement between the exact expression and approximation 1 outside the peaks (at 0 and at $0.5\lambda/d$, where d is size of a segment). Figure 3 right panel: there is almost no difference between approximation 1 and the Rician approximation up to $\sigma \approx 0.8$ rad; beyond this number Rician approximation saturates to the wrong value. Approximation 1 gives the correct saturation value. Both approximations work as long as $\sigma < \lambda/8$, i.e. for Strehl ratios higher than 50%.

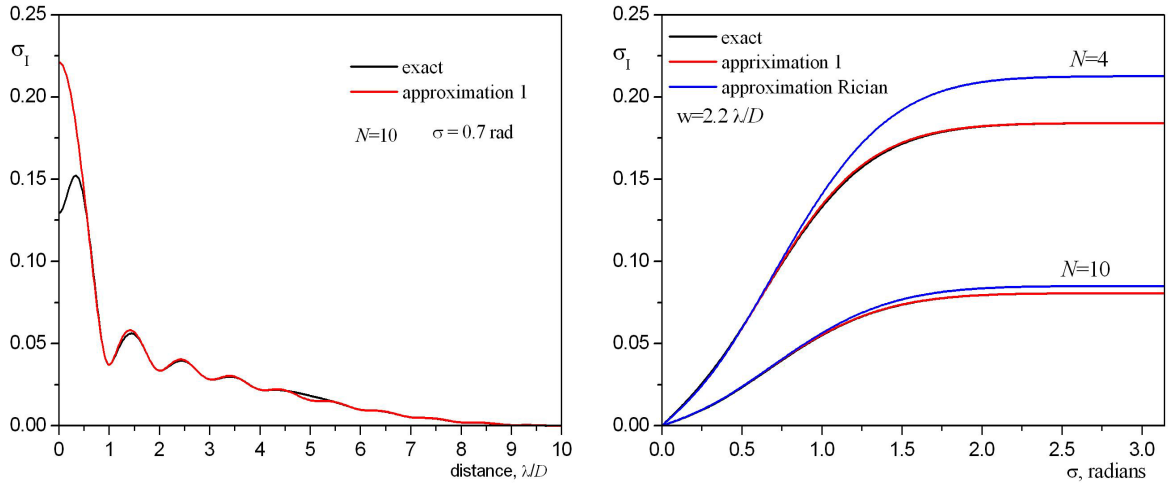

Figure 3. Standard deviation of intensity: exact expression, Eq.(12) (black), approximation 1, Eq.(15) (red), and the Rician approximation, Eq.(16) (blue). Left panel: angular dependence. There is no discernible difference between the two approximations for the case presented in the left panel, i.e. for σ = 0.7rad, and for this reason we did not plot the Rician approximation there. Right panel: dependence on the phase error rms value. *D* – pupil diameter, λ - wavelength. All curves are computed for a one-dimensional telescope.

2.3.2. *Central point*

At the central point $gf(0)=t(0)=1$, function $I_c = a_1^2$ is independent of N, and $I_s = \left(1-a_1^2\right)/N$. In order to have the same N^{-3} precision we need to keep all the terms. Eq.(12) can be re-written as

$$\sigma_I^2(0) = I_s^2 - NI_s^4 + 2I_cI_s - 4I_cI_s^2 - 2I_c^2I_s + I_c^2I_s^2 \tag{17}$$

Rician approximation, Eq.(16), does not work here: the term $2I_cI_s$ has the same σ^2N^{-1} dependence as the term $2I_c^2I_s$, so we cannot keep one without keeping another. In the same manner, terms $4I_cI_s^2$ and $I_c^2I_s^2$ have the same σ^4N^{-2} dependence as the term I_s^2, so all three have to be kept or removed simultaneously. If we keep only the σ^2N^{-1} terms the expression can be simplified:

$$\sigma_I^2(0) \approx 2I_cI_s(1-I_c) \tag{18}$$

By construction this approximation works only for large N and small σ. For large σ, when the difference between all the points of the image is smeared, Eq.(16) can be used for the central point. Figure 4 shows the exact curve, and the two approximations for standard deviation of intensity in the central peak.

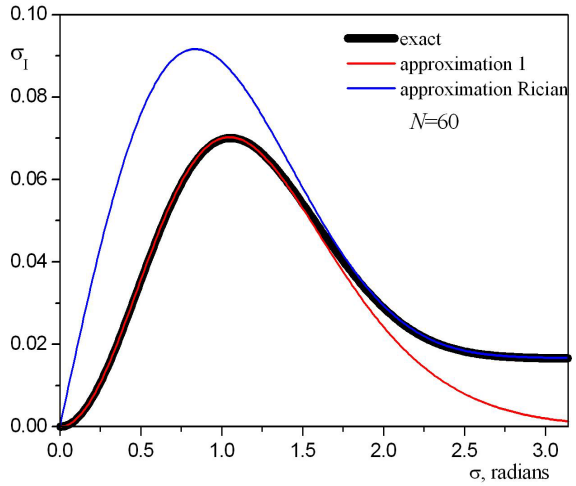

Figure 4. Standard deviation of intensity at the central point and the diffraction peaks (black). N=60 (1D case). Rician approximation (blue) provides a good fit only for large σ. For $\sigma < \lambda/4$ Eq.(18) provides a good fit (red), while Rician approximation is inapplicable.

As a side remark we want to mention that the curves in Figure 4 can be used to predict the performance of "lucky imaging" across the range of Strehl ratios delivered by compensated telescopes.[10]

2.3.3. *Diffraction peaks*

If the mirror surface is affected by piston aberrations only and if there are no gaps between segments then $t(\boldsymbol{w}_{peak})=0$. The intensity in these points is also zero. If there are some additional aberrations as, for example, segments' tip-tilt or defocus and/or the segments have gaps between them $t(\boldsymbol{w}_{peak})\neq 0$ and $gf(w_{peak})=1$. We introduce $I_{peak} = \left|t(\boldsymbol{w}_{peak})\right|^2$ – intensity of the peaks in the absence of piston errors. From Eq.(3) we see that $I_c(\boldsymbol{w}_{peak}) = I_{peak}I_c(0)$ and $I_s(\boldsymbol{w}_{peak}) = I_{peak}I_s(0)$. From Eqs. (2) and (12), keeping in mind that $gf(\boldsymbol{w}_{peak}) = gf(2\boldsymbol{w}_{peak}) = 1$ we obtain:

$$\langle I\rangle(\boldsymbol{w}_{peak}) = I_{peak}\langle I\rangle(0), \quad \sigma_I(\boldsymbol{w}_{peak}) = I_{peak}\sigma_I(0). \tag{19}$$

In the diffraction peaks mean and standard deviation of intensity are normalized versions of their counterparts in the central peak. All set above concerning the central peak is valid for the diffraction peaks taking into account a normalization factor. Contrast in the diffraction peaks is equal to contrast in the central peak:

$$C(\boldsymbol{w}_{peak}) = \frac{\sigma_I(\boldsymbol{w}_{peak})}{\langle I\rangle(\boldsymbol{w}_{peak})} = \frac{\sigma_I(0)}{\langle I\rangle(0)} = C(0). \tag{20}$$

3. STOCHASTIC SPECKLE DISCRIMINATION

3.1. Introduction

Consider a star-companion system seen through a segmented telescope. The companion looks like a speckle, but its intensity follows the statistics of the central peak of the PSF, while the speckle's intensity behaves as an off-axis point of the PSF (unless it is the diffraction peak which then behaves similarly to the central peak too – see Eq. (20)). To distinguish between speckle and the companion we calculate the inverse of variability for each pixel on a set of images. This method has been proven on real adaptive-optics images for non-segmented telescopes (Figure 5).[11] Below we calculated the efficiency of SSD for segmented pupils.

If during two sequential exposures the configuration of segments changes sufficiently the corresponding images represent two independent realizations of the intensity field. We utilize the intensity statistics rather than the integral intensity. If we assume that the phase errors are small, we expect the variability of a candidate source to be less than the variability of a speckle.

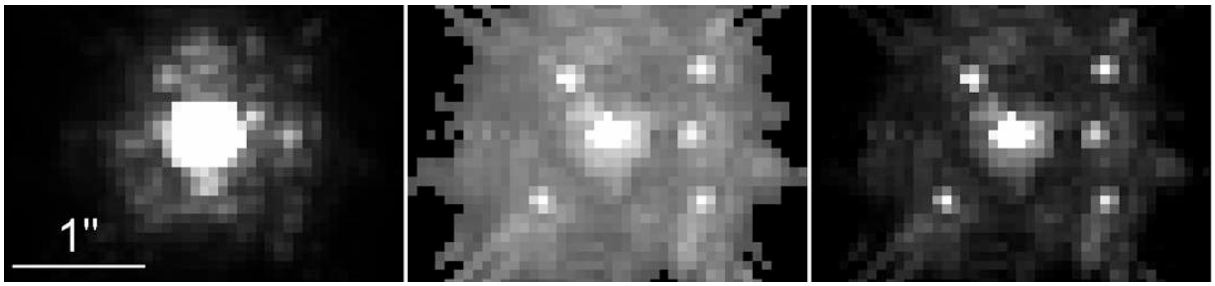

Figure 5. Demonstration of the SSD method on adaptive-optics data recorded with the 3m Shane Telescope at the Lick Observatory. Five artificial companions were inserted in the dataset. Left: shift-and-add image, center: SNR-map, right: beam ratio map. Strehl ratio was 50%. Images are displayed on the linear scale; the central parts are deliberately saturated to bring out the faint speckle structure outside the PSF core.

3.2. Signal-to-noise discrimination metric

One of the possible metrics for planet-speckle discrimination is signal-to-noise ratio (SNR):

$$SNR = \langle I \rangle / \sigma_I \,. \tag{21}$$

For SSD method to work SNR for the central point must be higher than for the speckles. Looking at Equations (3) and (8) we notice than SNR is independent of the segments' shape. The efficiency of SSD based on the SNR metric is:

$$E_{SNR} = \frac{SNR(0)}{SNR(\boldsymbol{w})} = \frac{\langle I \rangle(0)/\sigma_I(0)}{\langle I \rangle(\boldsymbol{w})/\sigma_I(\boldsymbol{w})}. \tag{22}$$

Basically E_{SNR} is equivalent to speckle contrast normalized by its value at the origin. Figure 6 shows E_{SNR} for a one-dimensional telescope. Left panel: E_{SNR} is higher between the rings of the diffraction-limited PSF. On the rings E_{SNR} is lower. It is not surprising because the presence of the non-negligible deterministic part of the PSF makes $SNR(\boldsymbol{w})$ larger. Between the rings, as well as for large angular distances E_{SNR} is maximal and constant. In these areas the deterministic part of the PSF is zero, and it is easy to show that speckle contrast and hence SNR is independent of the position in the focal plane. By definition, because we neglect the speckle contribution under the planet, its signal-to-noise ratio is $SNR(0)$ and it does not change with position. Therefore oscillations in the curves are the result of change in $SNR(\boldsymbol{w})$ only. Maximum value of E_{SNR} is obtained for the smallest value of $SNR(\boldsymbol{w})$ because $SNR(0)$ is constant. To obtain this minimum value for $SNR(\boldsymbol{w})$ we limit ourselves to normal distribution of segments' errors and substitute $I_c(\boldsymbol{w}) = 0$ in Equations (2) and (12).

$$SNR(\boldsymbol{w})_{\min} = \left[1 - \left(1 - a_1^2\right)^2 / N\right]^{-1/2}. \tag{23}$$

The corresponding maximum in E_{SNR} is computed with the help of Equations (5) and (11) (assuming Gaussian statistics for phase errors):

$$E_{SNR,\max} = \frac{1 - a_1^2 + N a_1^2}{\left(1 - a_1^2\right)\sqrt{N-1}} \sqrt{\frac{N - 1 + 2a_1^2 - a_1^4}{2N a_1^2 + 1 - 2a_1^2 + a_1^4}}. \tag{24}$$

where $a_1^2 = \exp(-\sigma^2)$. $E_{SNR,\max}$ is increasing with N, demonstrating that increasing the number of segments improves the efficiency of SSD. For large N one can use the following asymptotic:

$$E_{SNR,\max} \approx \frac{1}{\sqrt{2}} \frac{a_1}{1 - a_1^2} \sqrt{N}, \quad N >> 1. \tag{25}$$

$E_{SNR,\max}$ drops fast with σ (Figure 6 , right panel). We wish to know a limiting value of σ for which $E_{SNR,\max}$ is higher than a certain level M. Solving Eq.(25) with respect to a_1^2 we obtain:

$$e^{-\sigma_{\max}^2} \approx 1 + \frac{N}{4M^2} - \sqrt{\frac{N}{4M^2}} \sqrt{\frac{N}{4M^2} + 2}. \tag{26}$$

Putting for example $M = 10$ results in $\sigma_{max} = 0.7$rad (when $N = 50$), $\sigma_{max} = 0.83$rad (when $N = 100$), and $\sigma_{max} = 1.4$rad (when $N = 10000$). That is denser segmentation permits higher phase errors at which SSD still works.

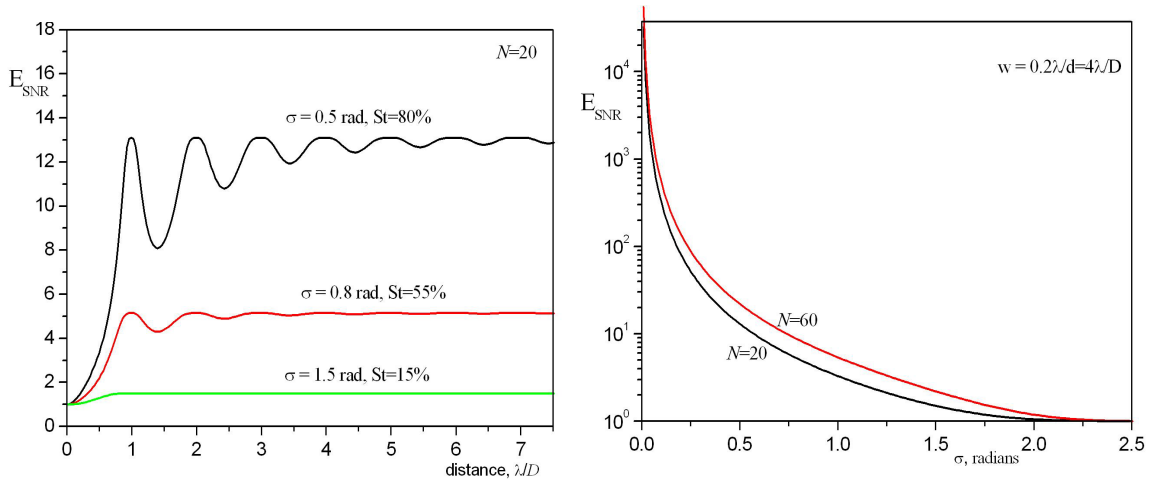

Figure 6. Efficiency of SSD based on the signal-to-noise metric. Left panel: angular dependence. Right panel: dependence on the phase error's standard deviation. *D* – pupil diameter, λ - wavelength, one-dimensional case.

3.3. Beam ratio discrimination metric

Another metric is the so called "beam ratio" usually denoted as r. On the set of images it is calculated from mean and standard deviation:[11]

$$r = \frac{\sqrt{\langle I \rangle^2 - \sigma_I^2}}{\langle I \rangle - \sqrt{\langle I \rangle^2 - \sigma_I^2}}. \tag{27}$$

It is easy to show that the two metrics are related:

$$r = \frac{\sqrt{SNR^2 - 1}}{SNR - \sqrt{SNR^2 - 1}}. \tag{28}$$

The efficiency of the beam ratio metric is again defined as the ratio of its value in the central peak to its off-axis value:

$$E_r = \frac{r(0)}{r(\boldsymbol{w})}. \tag{29}$$

The metric is constructed so that for the modified Rician distribution (see Eq.(16)) it equals $I_c(\boldsymbol{w})/I_s(\boldsymbol{w})$. For Rician distribution the theoretical efficiency of the beam ratio metric between the rings of the diffraction-limited PSF (where $I_c(\boldsymbol{w}) = 0$) is infinite. For a limited number of segments, where $\sigma_I(\boldsymbol{w})$ follows Eq.(15), E_r between diffraction rings is less than infinity, but still much higher than E_{SNR} (see Figure 7, unlike Figure 6 it has a logarithmic scale). E_r oscillates much stronger in the field than E_{SNR}: the difference between the on- and the off-ring positions is 1-2 orders of magnitude.

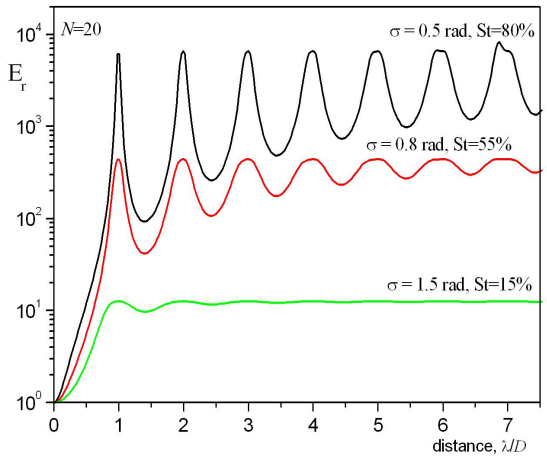

Figure 7. Efficiency of the SSD method based on the beam ratio metric. *D* – pupil diameter, λ - wavelength, one-dimensional telescope.

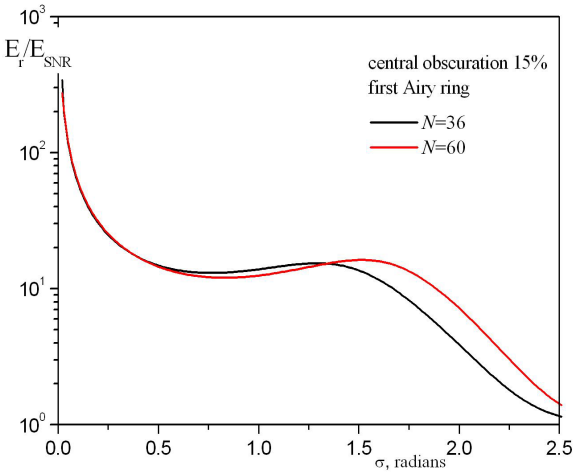

Figure 8. Ratio between the two metrics for the first Airy ring of a two-dimensional circular telescope with 15% linear obscuration ratio and hexagonal segments.

Obviously E_r is the preferred metric for detection between the rings. It is interesting to compare these two metrics for the position on top of a ring, i.e. in the minima of E_r and E_{SNR} which corresponds to the maxima of $I_c(\boldsymbol{w})$. For that we consider a circular telescope with diameter D and a central obscuration of size $0.15D$. The position of the first Airy ring is $1.63\lambda/D$. The value of the diffraction-limited PSF at this point is 0.0245. We assume that this pupil is composed of hexagonal segments. On the fist Airy ring the segment PSF can be approximated as[5]

$$\left|t(\boldsymbol{w})\right|^2 \approx 1 - \frac{5}{18}\frac{\pi^2 w^2}{N} + \frac{209}{6480}\frac{\pi^4 w^4}{N^2} \tag{30}$$

where w is modulus of $\boldsymbol{w}$ in λ/D units. Substituting $w = 1.63$ for the first Airy ring we obtain

$$I_c(\boldsymbol{w}_1) = 0.0245\, a_1^2, \qquad I_s(\boldsymbol{w}_1) \approx \frac{1-a_1^2}{N}\left(1 - \frac{7.28}{N} + \frac{22.18}{N^2}\right). \tag{31}$$

Substituting Eq.(31) into Equations (2) and (15) we calculate the moments and afterwards the metrics. The ratio E_r/E_{SNR} for the first Airy ring is plotted in Figure 8. Here the beam ratio metric also works better. Notice that for a range of σ from 0.5 to 1.5rad the ratio is practically constant and it equals approximately 14.

4. DISCUSSION

We obtained general expressions for the mean and standard deviation of intensity when the image is formed by a segmented pupil. The two moments can be expressed through the normalized diffraction-limited PSF for the whole pupil and the PSF for a single segment. The moments behave differently depending whether the considered point in the field falls on locations of the peaks or on another location. In a limit of large number of segments the standard deviation of the off-peak intensity can be approximated by the expression obtained from the modified Rician distribution. Nevertheless we did not prove that in this case the intensity distribution *is* modified Rician. Standard deviation of central point and diffraction peaks' intensity cannot be approximated by this expression, which proves that the intensity at these points *does not* follow the modified Rician distribution.

Based on the developed formulas we calculated two metrics for stochastic speckle discrimination: signal-to-noise and beam ratio. We find that even on top of the Airy rings beam ratio provides better results than signal-to-noise.

In the paper we considered statistics of the image formed by a segmented pupil. Nevertheless, often in literature the residual wavefront after adaptive optics (AO) correction is considered as being composed of a large number of independent cells.[12] To some extent the phase within a cell can be considered constant. The size of a cell is defined by a correlation length of the phase, which is related to inter-actuator distance. The actuators geometry is usually square. The diffraction peaks of the grid factor correspond to the so-called "waffle mode". This representation is especially valid for a high order AO with large number of actuators (extreme adaptive optics). Figure 9 shows the reconstructed wavefront from High Order Testbench (HOT)[13] with residual wavefront *rms* value of 40nm and the Strehl ratio of 88%. The phase errors are created by artificial turbulence. The cells of the wavefront are clearly seen. Based on this observation we claim that the material presented in this paper is equally valid for the residual phase after AO correction. The expressions and approximations for statistical moments, as well as for the SSD metrics are applicable to this type of images.

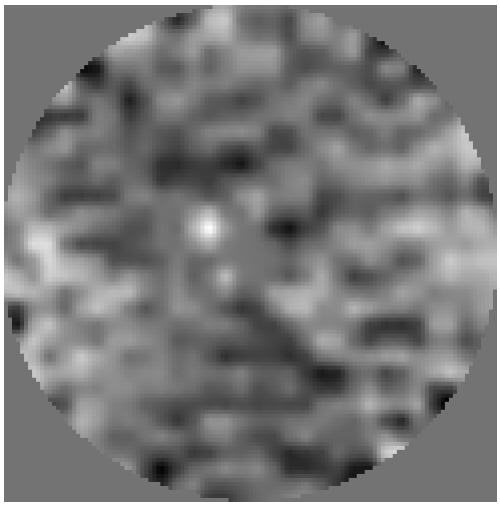

Figure 9. Reconstructed wavefront from the High Order Testbench, after AO compensation. Strehl ratio = 88%.

ACKNOWLEDGEMENTS

Effort sponsored by the Air Force Office of Scientific Research, Air Force Materiel Command, USAF, under grant number FA8655-09-1-3052. The U.S Government is authorized to reproduce and distribute reprints for Governmental purpose notwithstanding any copyright notation thereon.

REFERENCES

1. J.E. Nelson et al, "The Design of the Keck Observatory and Telescope," Keck Observatory Report No. 90 (1985)
2. P. Alvarez et al, "The GTC project: under commissioning," Proc. SPIE 7012 (2008)
3. R. Gilmozzi and J. Spyromilio, "The 42.5 m European ELT: status," Proc. SPIE 7012 (2008)

4. J. Nelson and G.H. Sanders, “The status of the Thirty Meter Telescope project,” Proc. SPIE 7012 (2008)
5. N. Yaitskova, K. Dohlen, and P. Dierickx, “Analytical study of diffraction effects in extremely large segmented telescopes,” J. Opt. Soc. Am. A **20**, 1563-1575 (2003)
6. S. Gladysz, N. Yaitskova, and J. Christou, “Statistics of Intensity in Adaptive-Optics Images and Their Usefulness for Detection and Photometry of Exoplanets,” accepted for JOSAA
7. N. Yaitskova, “Diffraction halo by a segmented telescope,” Proc. SPIE **7012**, (2008)
8. J. Goodman, “Speckle phenomena in optics: theory and applications” (Ben Roberts and Company, Englewood, Colorado, 2006)
9. J. Goodman, "Speckle with a finite number of steps," Appl. Opt. **47**, A111-A118 (2008)
10. S. Gladysz, J. C. Christou, N. M. Law, R. Dekany, M. Redfern, and C. D. Mackay, “Lucky imaging and speckle discrimination for the detection of faint companions with adaptive optics,” Proc. SPIE 7105, 70152H (2008)
11. S. Gladysz and J. Christou, “Reference-less detection, astrometry, and photometry of faint companions with adaptive optics,” The Astrophysical Journal **698**, 28-42 (2009)
12. V. Canales and M. Cagigal, “Rician Distribution to Describe Speckle Statistics in Adaptive Optics,” Appl. Opt. **38**, 766-771 (1999)
13. E. Aller-Carpentier et al. “High order test bench for extreme adaptive optics system optimization,” Proc. SPIE, Vol. 7015, (2008)